Cite as: Sokolov M., Franciosa P., Al Botros R., Ceglarek D., Keyhole Mapping to Enable Closed-loop Weld Penetration Depth Control for Remote Laser Welding of Aluminum Components using Optical Coherence Tomography, Journal of Laser Applications 32 (3), 032004,2020.

KEYHOLE MAPPING TO ENABLE CLOSED-LOOP WELD PENETRATION DEPTH CONTROL FOR REMOTE LASER WELDING OF ALUMINIUM COMPONENTS USING OPTICAL COHERENCE TOMOGRAPHY

Paper #Macro 1602

Mikhail Sokolov, Pasquale Franciosa, Rehab Al Botros, Darek Ceglarek

WMG, University of Warwick, Gibbet Hill Road, Coventry CV4 7AL, UK

Abstract

Remote Laser Welding (RLW) combines the positive features of tactile laser welding with additional benefits such as increased processing speed, reduced operational cost and service as well as higher process flexibility. A leading challenge preventing the full uptake of RLW technology in industry is the lack of efficient Closed Loop In-Process (CLIP) monitoring and weld quality control solutions. This underpins the need to fuse multiple sensor technologies, data analytics along with predictive engineering simulations. Although the development and integration of a variety of sensors, covering the radiation spectrum from ultra-violet to far-infrared, the flawless deployment of CLIP solutions is still challenged by the need for: signal de-noising in case of process instability; real-time data analytics; adaptive control engineering architecture to cope with process variations induced by manufacturing tolerances.

This paper focuses on the aspect of the Weld Penetration Depth Control (WPDC) using Optical Coherence Tomography (OCT) as necessary step to enable adaptive penetration depth control during RLW of aluminium components in fillet lap joint configuration in consideration of part-to-part gap variation. The approach is decoupling the welding process parameters in two sub-sets: (1) in-plane control of the heat input on the upper part to facilitate the droplet formation; (2) out-of-plane heat management to achieve the desired level of penetration control in keyhole mode. The paper presents the results of the keyhole mapping with variable part-to-part gap, that provide the insights for future research to enable the fully automatic closed-loop weld penetration depth control. Current limitations and next phases of research and development are highlighted based on the experimental study.

Keywords: Remote Laser Welding, Aluminium Alloy, Fillet Lap Joint, Optical Coherence Tomography, Gap Bridging, Keyhole Mapping

Introduction

Remote Laser Welding (RLW) applications of aluminium components in automotive industry is monotonically increasing, driven by the continuous effort for light-weight body construction and the recent market push for battery electric vehicles with un-precedent need for aluminium structures which are key elements for battery tab assembly, electrical drive components, structural battery casing/frames and underbody [1].

Compared to steel or ferrous-based alloys, welding of aluminium structures poses key challenges due to the low viscosity of the molten liquid which leads to reduced process window and higher probability of weld defects because of fast collapse of the keyhole [2]. In recent years, most of the research effort has been devoted to develop effective solutions to improve the keyhole stability and maximise the weldability of aluminium alloys. This has been possible with the introduction of laser beam oscillation and power modulation techniques. Recently, Müller et al. [3] and Franciosa et al. [4] described how laser beam oscillation can be used to enable part-to-part gap bridging in fillet lap joints. The latter study highlighted the benefits of switching from overlap seam welding to fillet lap welding with a weight saving up to 4.5 kg per car, and capability for adaptive in-process gap bridging. Optimal process window selection and robust process parameters through necessary steps are not sufficient enough to guarantee defect-free welds in presence of process variability and manufacturing tolerances. Closed Loop In-Process (CLIP) monitoring and quality control strategy is therefore envisaged to guarantee the fulfilment of the multiple requirements, such as mechanical, thermal and electrical as dictated for example by new emerging battery assembly systems [5].

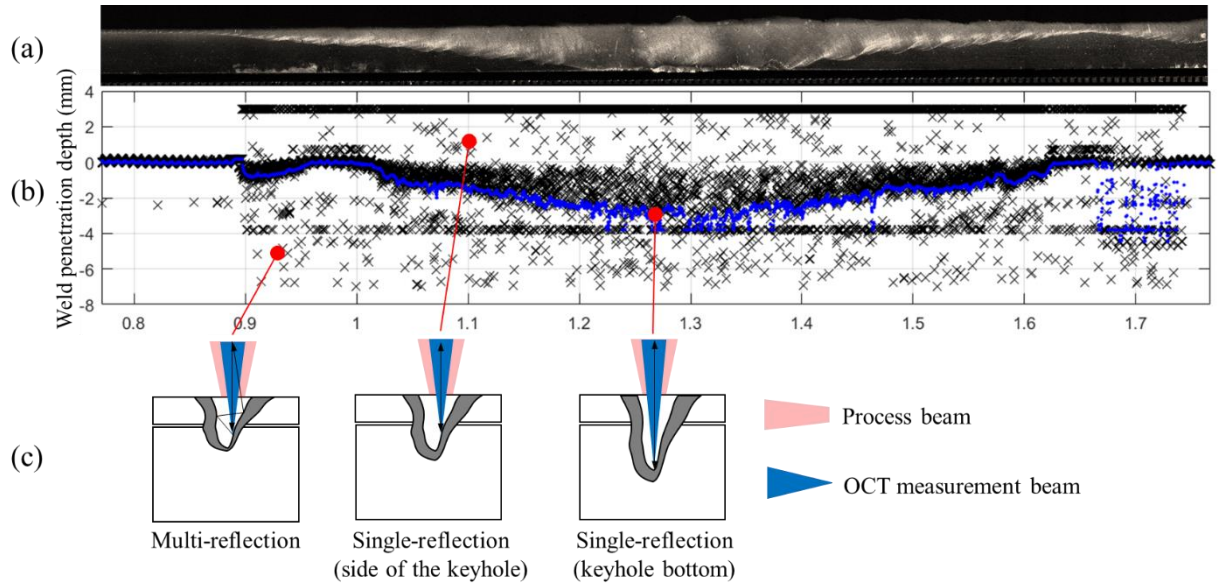

Figure 1 OCT signal interpretation: (a) longitudinal cross-section of weld;
(b) raw (black cross) and processed (blue dot) OCT signal; (c) reflection modes and interpretations.

Among all, weld penetration depth plays a key role to deliver weld quality, as discussed in [6, 7, 8]. For example, in case of battery case welding, the welding process needs to be controlled to provide required weld characteristics without penetrating the battery case [9]; whereas lack of penetration in battery tab causes insufficient contact area, which leads to voltage drop and consequent malfunction of the whole battery pack. To keep weld penetration depth within the required limits, an in-process Weld Penetration Depth Control (WPDC) system needs to be integrated within the CLIP quality control module.

To date, only a limited number of WPDC methods have been developed. Most of those methods are based on indirect signals and data, such as process emissions, gathered with photodiode-based monitoring systems. The generated emissions are converted into electrical signals by photodiodes along with an optical filters. Key features, such as plasma temperature, reflected laser intensity, and plasma intensity, are predefined for a good quality weld and associated to a reference signal and predictive models are build using multi-variate statistics [10]. Though those approaches are the state-of-art today for correlation and trend analysis they suffer the possibility to be extended outside of the training dataset. This translates to the fact that any process change or process variability, such as part-to-part gap or seam misalignments, cannot be handled.

In-process quality control formed the central focus of a study by You et al. [11] in which authors used five types of sensors for laser welding process monitoring and X-ray imaging was used for keyhole depth monitoring. Bautze et al. [7] compared multiple approaches of laser welding monitoring and control, and concluded that due to intense process emissions and extreme temperature gradients, as well as highly unstable process states in case of laser welding of aluminium, the only monitoring technique that can provide direct and in-process measurement of the keyhole depth is Optical Coherence Tomography (OCT).

With OCT light reflections are measured by the Michelson interferometer, using the low coherence properties of a broadband laser source. The key principle is the comparison between the travel lengths of the reflections of the measurement laser beam directed towards the keyhole bottom with that of a reference laser beam inside the interferometer. Any change in the keyhole wall or depth will generate interference fringes which are translated, using fast Fourier transform (FFT) filters, into distance measurement [12]. Figure 1 shows a typical OCT signal obtained with a power ramp of the process beam, in overlap seam welding. When the OCT measurement beam is correctly aligned towards the keyhole bottom, the OCT technology is capable of providing fast and accurate direct measurement of the keyhole depth. Assuming that the molten layer just underneath the keyhole bottom is neglectable, this approach results in a promising solution for WPDC. OCT technology has been successfully used for continuous monitoring of weld penetration depth in a number of applications, primarily with stationary process beam and overlap seam welding. Few studies have examined the

opportunity of utilizing OCT for WPDC with application to aluminium alloys. According to Bautze et al. [7] laser welding of aluminium alloys requires ad-hoc data analytics approaches as the keyhole oscillates at high frequency (typically between 1 to 5 kHz), which induces noise into the OCT signal. Comparing OCT signals during laser welding of mild steel and aluminium alloy, the authors noticed that in case of aluminium the signal has a wider variance and proposed that signal's variance can be used to determine the process window. Comparing OCT sensor signal with X-ray, Fetzer et al. [13] used 80th percentile filter with a 1.0 ms symmetrically placed window as it resulted in a minimal deviation between the depth measured with both methods. Kogel-Hollacher et al. [14] used two measurement beams ("TwinTec" module): one towards the keyhole and the second focused on the base material surface to get the precise weld penetration depth value as a result of subtraction of these two signals. In later research Kogel-Hollacher et al. [15] applied low-pass filter to compensate high frequency keyhole oscillations in welding of aluminium. Experimental results by Dorsh et al. [8, 16] show that the OCT measurement beam, targeting the bottom of the keyhole, has to be properly aligned with respect to the keyhole shape and such alignment is not universal and has to be adjusted for every specific welding task. After comparing signals from copper and aluminium alloys, Schmoeller et al. [17] suggested that differences in statistical parameters of OCT signals are caused by material-dependent geometry of the keyhole, as aluminium has a tendency to form a conical geometry of the keyhole, while copper alloys show a bottle-shaped geometry and this causes different reflection patterns. This conclusion renews the interest in keyhole shapes research and classification models developed in [18, 19] as well as analytical approach suggested in [20, 21].

This paper contributes to develop the necessary step to enable WPDC during RLW process of aluminium components with fillet lap joint configuration and in consideration of part-to-part gap bridging control. The paper is underpinned by the key observation that the weld penetration control is intrinsically coupled to the gap bridging. This problem is tackled by decoupling the welding process parameters in two sub-sets: in-plane control of the heat input on the upper part to facilitate the droplet formation, and therefore reach gap bridging; out-of-plane heat management to achieve the desired level of penetration control in keyhole mode. The results of the keyhole mapping with variable part-to-part gap conditions are presented in the form of a set of "mapping charts" which help to select the optimal alignment of the OCT measurement beam. The fundamental steps to compute the mapping charts are discussed and illustrated throughout the paper.

Materials and methods

Experimental configuration

The material used in the welding experiments with a CW multi-mode diode laser (LDF 6000-6 LaserLine GmbH, Germany) was SSR 5182 Aluminium (4.3% Mg) in single fillet lap joint configuration. The laser beam was delivered through an optical fiber of 150 μm diameter and coupled with the WeldMaster Scan&Track remote welding head (YW52 Precitec GmbH, Germany) and the In-process Depth Meter (IDM, Precitec GmbH, Germany) sensor.

List of equipment and parameters are shown in Table 1. All experiments were performed without shielding gas and without filler wire. Samples were wiped with acetone before welding to remove surface contaminations. The IDM sensor was installed just below the motorised collimator of the welding head. This allows to defocus the process laser beam independently of the OCT sensor. However, the measurement beam of the IDM was deflected and focused using the same motorised mirror and focusing unit of the main process beam.

Table 1 Specification of experimental setup.

Characteristics	**Value**
Welding laser: LDF 6000-6, LaserLine GmbH	
Operation mode	CW
Nominal output power (kW)	6
Emission wavelength (nm)	1080
Beam parameter product (mm · mrad)	6
Process fibre core diameter (μm)	150
Welding optics: YW52 WeldMaster, Precitec GmbH	
Collimating length (mm)	150
Focusing length (mm)	300
Focal spot diameter (mm)	0.3
Sensor: IDM, Precitec GmbH	
Sampling rate (kHz)	70
Emission wavelength (nm)	1550
Sensor beam maximum power (mW)	10
Sensor beam intensity (%)	30
Spot diameter (mm)	0.05
Max measurement range (mm)	10

Overview of proposed approach

The proposed CLIP approach is shown in Figure 2 and is discussed as follows: (1) part-to-part gap bridging (QL[1]) with adaptive selection and adjustment of welding process parameters, via beam oscillation and power modulation. Details about QL[1] are described in [4]; (2) weld penetration depth monitoring and control using OCT technology (QL[2]).

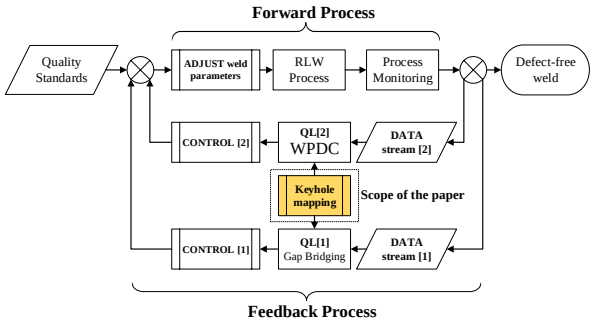

Figure 2 Closed-Loop quality control system for RLW process for gap bridging and weld penetration control.

QL[1] and QL[2] are mutually coupled. For example, the weld may exhibit poor bonding (i.e., no gap bridging) as illustrated in Figure 3 (a), and yet a satisfactory weld penetration is achieved; controversially, poor penetration can be reached though very sound bonding condition is achieved as in Figure 3 (b).

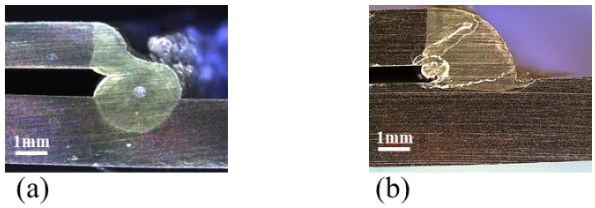

Figure 3 Coupling effect between QL[1] and QL[2].
(a) poor bonding and good penetration;
(b) good bonding and poor penetration.

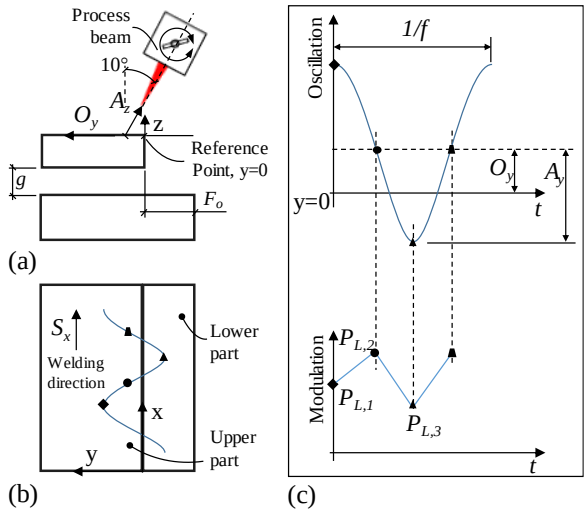

Figure 4 Definition of key welding process parameters Image adapted from [4].

Previous work [4] has shown that the weld parameters are as follows (see Figure 4): (1) laser power, P_L, which is modulated transversally to the welding direction; P_L is modulated on three points: $P_{L,1}$ to $P_{L,3}$, which correspond to the laser power on the upper part, reference point, and lower part, respectively; (2) oscillation amplitude, A_y, of the oscillation pattern with frequency f; (3) lateral offset, O_y – it is measured from the reference point, and defines the position in the y direction of the laser beam when A_y is zero; (4) focal point position offset, A_z - distance along the beam axis between the focal point and the intersection of laser beam with the part being welded.

In order to make the control architecture manageable and more intuitive, we have decoupled the welding process parameters in two sub-sets as follows:

(1) Parameters related to QL[1]: gap bridging is driven by the heat input generated in-plane. Key parameters are: A_y , O_y, A_z, $P_{L,1}$ and $P_{L,2}$
(2) Parameters related to QL[2]: $P_{L,2}$ and $P_{L,3}$ to control weld root and penetration depth.

This leaves only one single parameter, $P_{L,2}$, which is shared between QL[1] and QL[2].

QL[1]-related parameters are adaptively changed on the fly during welding using the linear control model stated in Equation (1), where g is the part-to-part gap measured using the seam tracking device; whereas the constants A_{Ay}, B_{Ay}, A_{Oy}, B_{Oy}, A_{Az}, B_{Az} and A_p are computed using the approach proposed in [4].

$$\begin{cases} A_y = A_{Ay} \cdot g + B_{Ay} \\ O_y = A_{Oy} \cdot g + B_{Oy} \\ A_z = A_{Az} \cdot g + B_{Az} \\ P_{L,i} = P_{L,i}^{(gap=0)} + A_{P,i} \cdot g, \forall i = 1,2 \end{cases} \quad (1)$$

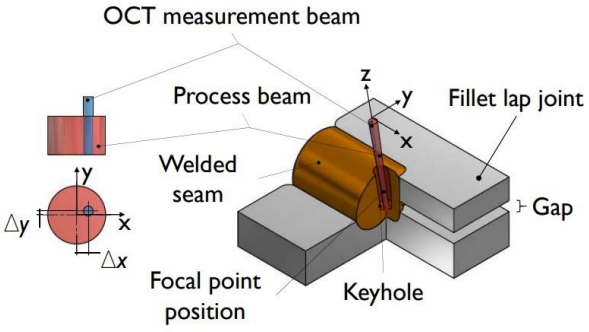

Figure 5 Conceptual representation of the alignment of the OCT measurement beam for fillet lap joint.

The paper aims at developing the keyhole mapping with variable part-to-part gap conditions in order to understand how the keyhole shape behaves in case of changes to process parameters, induced by variation of

part-to-part gap, as per Equation (1). The mapping is obtained by linking the relative position of the OCT measurement beam, defined by Δx and Δy, as illustrated in Figure 5, to the OCT signal. When Δx and Δy are zero the OCT measurement beam is perfectly aligned with the process beam. The relative positions were controlled by manually adjusting the beam deflection on the IDM collimator.

Keyhole mapping

The logical flowchart to compute the keyhole mapping is illustrated in Figure 6. The methodology comprises of three key steps and is iterated for each gap condition, from zero to the maximum bridgeable gap, g_{max}. We assume that g_{max} is 50% of the thickness of the upper material, as experimentally proved in [22] and then mathematically validated in [4].

STEP[1]: for the given gap condition (g), welding process parameters are computed in QL[1], as defined by Equation (1). The relative positions of the OCT measurement beam, Δx and Δy, are sampled within the minimum and maximum technology limits of the OCT collimator. We have assumed that those limits are capped by the focal spot diameter of the process beam. Resolution of data points around the bottom of the keyhole was increased.

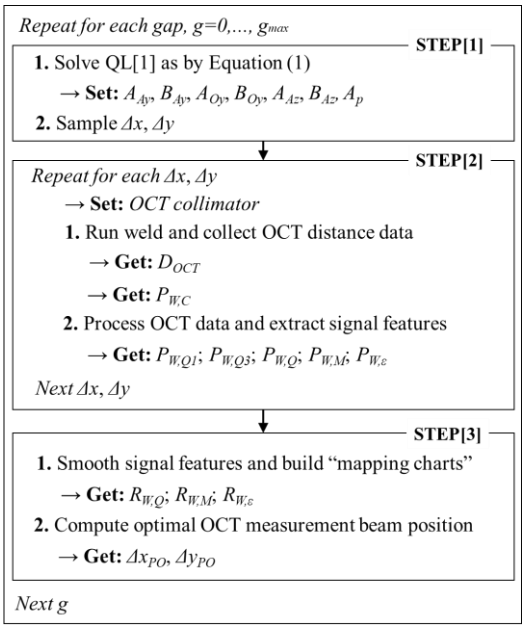

Figure 6 Proposed methodology for the computation of the keyhole mapping for variable part-to-part gaps.

STEP[2]: once OCT data, D_{OCT}, are collected for given gap and position of the OCT measurement beam, key signal features are extracted (see Figure 7). The approach uses a moving window which scans the whole signal and computes the following features:

(1) *Inter-quartile range*, $P_{W,Q3} - P_{W,Q1}$, corresponding to 75% ($P_{W,Q3}$) and 25% ($P_{W,Q1}$) percentiles, respectively, of the probability density function. The inter-quartile range is used as a measure of the signal spread. For instance, when the OCT measurement beam hits the un-molten surface, or the molten pool evolving in conduction mode, we expect low spread of the signal. Once the keyhole mode is established the spread tends to raise because of the multi-reflection within the keyhole. The variation in spread is therefore used to detect the start/end of the keyhole mode. We have not used a synchronised trigger with the power laser signal, because that would not allow to detect the exact transition to keyhole mode.

(2) *Weld penetration depth*, $P_{W,Q}$. Previous research has shown that 80% percentile results in the minimal deviation between $P_{W,Q}$ and the actual penetration depth, $P_{W,C}$, measured by cross-sections analysis. This result has been also confirmed for the current setup used in this paper. In order to compare $P_{W,Q}$ to the cross-section data, it has been subtracted with the value of the reference material surface.

(3) *Normalised modality index*, $P_{W,M}$. It is a normalised index in the range [0, 1] which describes the shape of the density function distribution. The shape of the density function is a key feature which gives insights about dynamics and shape of the keyhole. For instance, when the OCT measurement beam is positioned close to the keyhole bottom we expect a single-modal distribution, eventually skewed (Figure 8 (a)). If the OCT measurement beam is shifted toward the side of the keyhole and closer to the unmolten surface of the material (Figure 8 (b)), the distribution becomes bi-modal because of the reflections directly from the material surface. The same OCT's beam position could also capture fluctuations in the keyhole opening with eventually multiple humps on the wall of the keyhole; this leads to a multi-modal distribution (Figure 8 (c)).
The modality index ($P_{W,M}$) is computed using the Hartigans' Dip test, which measures the probability of observing a single-modal distribution. Therefore, the higher $P_{W,M}$ the higher the probability of obtaining single-modal distribution.

(4) *Normalised weld penetration depth accuracy*, $P_{W,\varepsilon}$. The accuracy of the measurement takes into account the combined effect of the process dynamics, which impacts the shape of the keyhole, and the sensor accuracy. $P_{W,\varepsilon}$ is a normalised index in the range [0, 1] and is computed by comparing the distribution of weld penetration depth, $P_{W,Q}$, against the actual distribution of weld depths measured with

metallographic analysis, $P_{W,C}$. The distribution of $P_{W,Q}$ is obtained by scanning the OCT data stream with a pre-defined set of moving windows. We have implemented the non-parametric Mann-Whitney test which determines whether $P_{W,Q}$ and $P_{W,C}$ are samples from the same distribution with equal medians. Therefore, higher values of $P_{W,\varepsilon}$ corresponds to higher level of weld penetration depth accuracy.

STEP[3]: the last step of the proposed methodology entails the approximations of the sampled signal features with a smooth analytical model. This is formulated as in Equation (2), where $R_{W,Q}^{(g)}$, $R_{W,M}^{(g)}$ and $R_{W,\varepsilon}^{(g)}$ are the approximation models that define the mapping charts for a specified gap (g).

$$\begin{cases} R_{W,Q}^{(g)} = f_{W,Q}^{(g)}(\Delta x, \Delta y) \\ R_{W,M}^{(g)} = f_{W,M}^{(g)}(\Delta x, \Delta y) \\ R_{W,\varepsilon}^{(g)} = f_{W,\varepsilon}^{(g)}(\Delta x, \Delta y) \end{cases} \quad (2)$$

Approximation models have been computed using the local regression weighted smoothing approach, with first order polynomial kernel. The optimal positions of the OCT measurement beam, Δx_{PO} and Δy_{PO}, are then evaluated by computing the maximum $R_{W,\varepsilon}^{(g)}$.

Results and key findings

Process parameters

Process parameters are listed in Table 2. The incidence angle of the process beam was constant and equal to 10°. Welding speed (S_x) and oscillation frequency (f) were set to 6 m/min and 150 Hz, respectively. The thickness of the test materials was 1.5 mm and 2.2 mm for the upper and lower part, respectively. The flange overlap (F_o) was 5mm.

Three levels of part-to-part gaps were analysed: 0.1±0.1mm; 0.35±0.1mm; 0.6±0.1mm. Part-to-part gap was set by calibrated shim packs (Meusburger Georg GmbH, Germany). Δx and Δy were sampled in the range [-0.18, 0.08] mm and [-0.11, 0.05] mm, respectively. OCT data streams were collected and exported from the IDM Explorer Software© and then processed in Matlab© to extract the signal features and compute the mapping charts. The moving scanning window was set with a width of 1 ms.

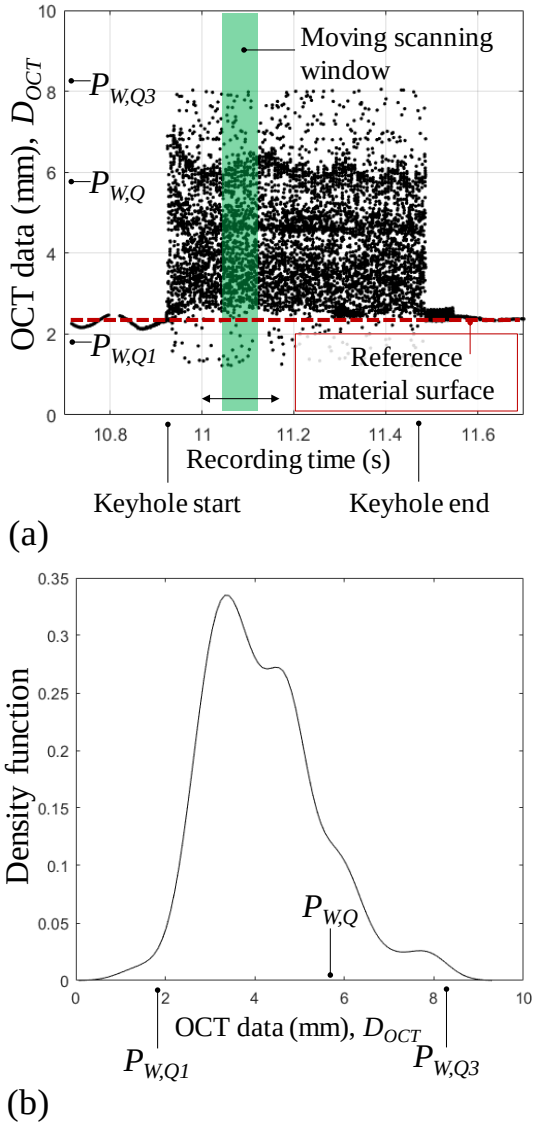

Figure 7 (a) Example of OCT data stream; (b) density function of the data points belonging to the moving scanning window shown in (a).

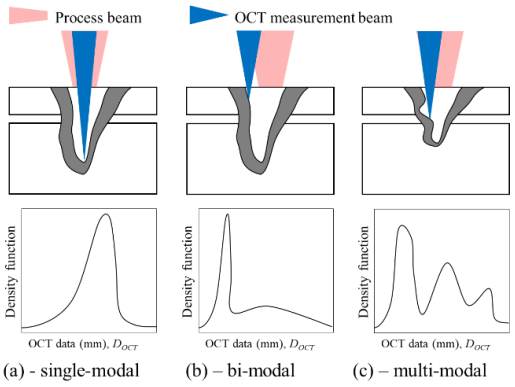

Figure 8 Interpretation of normalised modality index.

Table 2 Adopted process parameters for part-to-part gap bridging control.

Parameter	Value	Unit
A_{Ay}	0.75	--
B_{Ay}	1.50	mm
A_{Oy}	1.50	--
B_{Oy}	0.10	mm
A_{Az}	-4.10	--
B_{Az}	2.00	mm
$A_{p,1}$	1.10	kW/mm
$A_{p,2}$	0.61	kW/mm
$P_{L,1}^{(gap=0)}$	5.20	kW
$P_{L,2}^{(gap=0)}$	5.80	kW
$P_{L,3}$	2.30	kW

Key findings

Figure 9 and Figure 10 show the calculated mapping charts for the three selected part-to-part gap values. Results show that the keyhole gets deeper as the gap increases (see Figure 9 (a) and Figure 10 (b)). For instance the observed average weld penetration depth for g = 0.1 ± 0.1mm is about 2.3 mm; whereas it becomes about 3.0 mm for g = 0.6 ± 0.1 mm. This is explained by the fact that the gap bridging architecture defocuses the process beam inside the material surface to achieve stable droplet generation and bonding condition. The optimal positions of the OCT measurement beam are summarised in Table 3 and plotted in Figure 9 (c). Previous studies have concluded the OCT measurement beam needs to be re-adjusted in case of changes to process parameters. Our results show that when the OCT technology is used to measure weld penetration depth with integrated gap bridging control and adaptive changes of process parameters, we can use the same position (i.e., Δx_{PO} = 0 mm and Δy_{PO} = -0.03 mm) of the OCT measurement beam for gaps up to 0.4 mm. Only for larger gaps (> 0.5 mm) the optimal position of the OCT measurement beam drift towards the traversal y-axis.

Table 3 Optimal positions of the OCT measurement beam for different part-to-part gap values.

Part-to-part gap (mm)	Δx_{PO} (mm)	Δy_{PO} (mm)
0.10±0.1	0.0	-0.03
0.35±0.1	0.0	-0.03
0.60±0.1	0.0	-0.05

The shift in the optimal position of the OCT measurement beam is also supported by the fact that the shape of the keyhole tends to become narrower and slightly twisted when moving from g = 0.1 ± 0.1 mm to g = 0.6 ± 0.1 mm. This conclusion is clearly visible in the normalised modality index in Figure 9 (b) and Figure 10 (c) which show how the distribution of the OCT data changes towards a bi-modal distribution in correspondence of the optimal position of the OCT measurement beam, for g =0.6 ± 0.1 mm. The physical interpretation of the bi-modal distribution could be imputed to the appearance of a pronounced tail in the welded area, as illustrated in the metallographic cross-section in Figure 10 (a). The tail could be the result of the adaptive changes of the process parameters to react against the variation in gap.

Conclusions

This paper has contributed to develop the necessary step to enable closed-loop weld penetration depth control using OCT for RLW of aluminium components in fillet lap joint configuration and in consideration of part-to-part gap bridging control.

Though OCT has been widely deployment to a number of applications, the mechanisms that underpin OCT and RLW with beam oscillation and laser power modulation with the purpose of controlling part-to-part gap are not fully understood. The paper has been based on the assumption that dynamic changes to process parameters, as happening during gap bridging control, lead to re-adjustments of the OCT measurement beam because of variations to the keyhole shape.

The paper has developed a novel approach to systematically map the relative position of the OCT measurement beam for different values of part-to-part gap. OCT data has been parametrised with key features, which describe the shape and the depth of the keyhole.

Results have shown that, among all, the normalised modality index is the key parameter which must be monitored and controlled to detect and diagnose failures in weld penetration depth monitoring. Furthermore, statistical evidences have helped to conclude that robust control of weld penetration depth in filled weld configuration is viable for part-to-part gaps below 0.4 mm. Any bigger gap would need the implementation of an adaptive control architecture, with dynamic changes of the position of the OCT measurement beam.

Future work will focus on the developed of the closed-loop system to control the weld penetration depth.

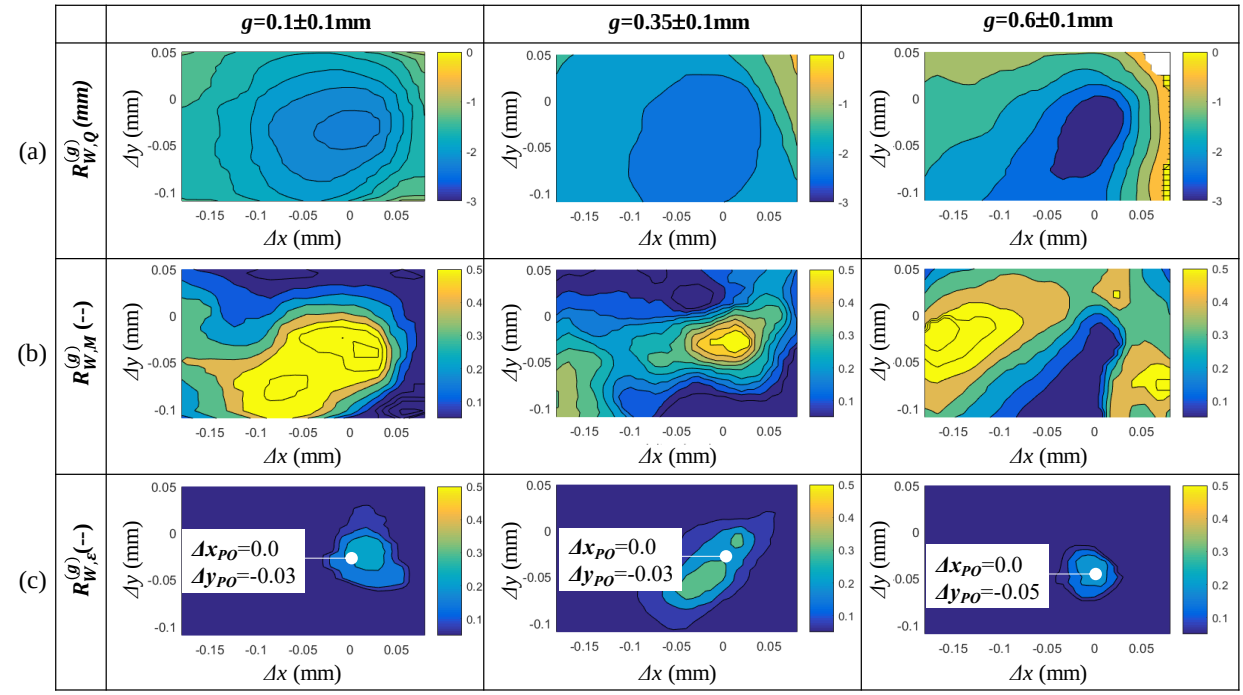

Figure 9 Mapping charts for different part-to-part gap values. (a) Weld penetration depth; (b) normalised modality index; (c) normalised weld penetration depth accuracy.

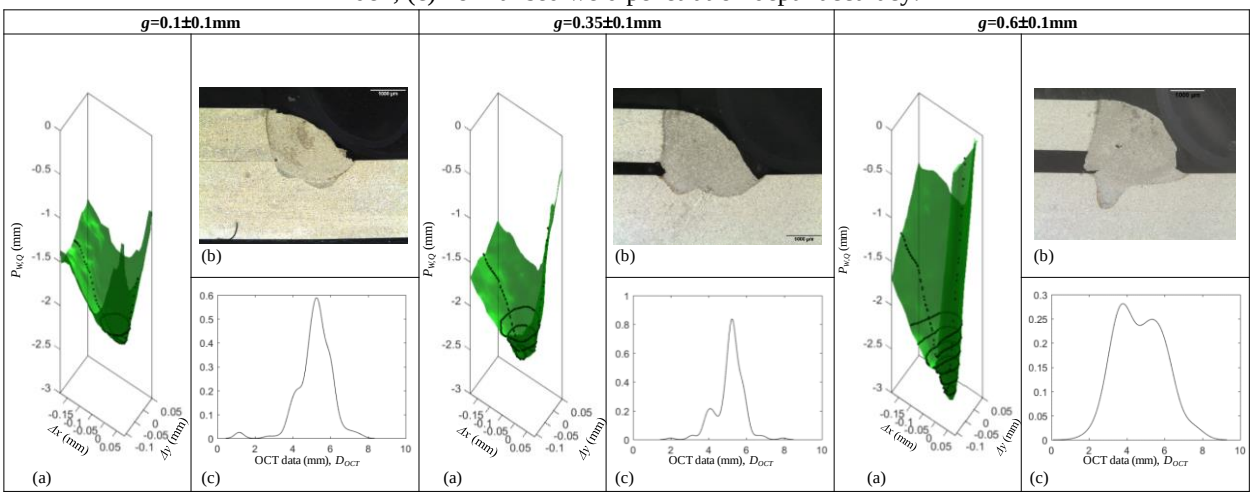

Figure 10 (a) Representative cross-section; (b) 3D view of the keyhole shape; (c) density function of OCT data

Nomenclature

A_{Ay}, A_{Az}, A_{Oy}, A_p	Experimentally computed welding constants for gap-bridging
B_{Ay}, B_{Az}, B_{Oy},	
A_y	Laser beam oscillation amplitude, mm
A_z	Focal point position offset, mm
D_{OCT}	Distance measured by OCT, mm
g, g_{max}	Part-to-part gap, mm
Oy	Laser beam lateral offset, mm
$P_{L,i}$	Laser power in point i, kW
$P_{W,C}$	Measured WPD at cross-section, mm
$P_{W,M}$	Normalized modality index, [0, 1]
$P_{W,Q}$	Measured WPD by OCT, mm
$P_{W,\varepsilon}$	Normalized WPD accuracy, [0, 1]
$R_{W,M}^{(g)}$ $R_{W,Q}^{(g)}$ $R_{W,\varepsilon}^{(g)}$	Approximation models for mapping for specified gap
Δx, Δy	Relative position of the OCT beam, mm
$\Delta x_{PO,}$ Δy_{PO}	Optimal position of the OCT beam, mm

Acknowledgements

This study was partially supported by the WMG Centre High Value Manufacturing Catapult (HVMC), APC UK project: Chamaeleon - New lightweight Materials and Processing Technologies for Common Lightweight Architecture of Electric and Hybrid Powertrain Systems, and the EPSRC UK project EP/K019368/1: Self-Resilient Reconfigurable Assembly Systems with In-process Quality Improvement. We acknowledge the technical support of Precitec GmbH, Gaggenau (Germany).

References

[1] Kölmel A., Sauer A. & Lanza G. (2014) Quality-oriented production planning of battery assembly systems for electric mobility, Procedia CIRP, 23, 149–154.

[2] Ceglarek, D., Colledani, M., Váncza, J., Kim, D.Y., Marine, C., Kogel-Hollacher, M., Mistry, A. & Bolognese, L. (2015) Rapid deployment of remote laser welding processes in automotive assembly systems, CIRP Annals, 64(1), 389-394.

[3] Müller, A., Goecke, S.F., Sievi, P., Albert, F. & Rethmeier, M. (2014) Laser beam oscillation strategies for fillet welds in lap joints, Physics Procedia, 56, 458-466.

[4] Franciosa, P., Serino, A., Botros, R.A. & Ceglarek, D. (2019) Closed-loop gap bridging control for remote laser welding of aluminum components based on first principle energy and mass balance, Journal of Laser Applications, 31(2), 022416.

[5] Dorsch, F., Dubitzky, W., Effing, L., Haug, P., Hermani, J.P. & Plasswich, S. (2017) Capillary depth measurement for process control, in High-Power Laser Materials Processing: Applications, Diagnostics, and Systems VI, San-Francisco, USA, 1009708

[6] Bautze, T., Moser, R., Strebel, M. and Kogel-Hollacher, M. (2015) Use of inline coherent imaging for laser welding processes: Process control and beyond, In Lasers in Manufacturing Conference, Munich, Germany.

[7] Bautze, T. & Kogel-Hollacher, M. (2014) Keyhole Depth is just a Distance: The IDM sensor improves laser welding processes, Laser Technik Journal, 11(4), 39-43.

[8] Das, A., Li, D., Williams, D. & Greenwood, D. (2018) Joining technologies for automotive battery systems manufacturing, World Electric Vehicle Journal, 9(2), 22.

[9] Ozkat, E.C., Franciosa, P. & Ceglarek, D. (2017) Development of decoupled multi-physics simulation for laser lap welding considering part-to-part gap, Journal of Laser Applications, 29(2), 022423.

[10] You, D., Gao, X. & Katayama, S. (2015) Detection of imperfection formation in disk laser welding using multiple on-line measurements, Journal of Materials Processing Technology, 219, 209-220.

[11] Webster, P.J., Wright, L.G., Mortimer, K.D., Leung, B.Y., Yu, J.X. & Fraser, J.M. (2011) Automatic real-time guidance of laser machining with inline coherent imaging, Journal of Laser Applications, 23(2), 022001.

[12] Webster, P.J., Wright, L.G., Ji, Y., Galbraith, C.M., Kinross, A.W., Van Vlack, C. & Fraser, J.M. (2014) Automatic laser welding and milling with in situ inline coherent imaging, Optics letters, 39(21), 6217-6220.

[13] Fetzer, F., Boley, M., Weber, R. & Graf, T. (2017) Comprehensive analysis of the capillary depth in deep penetration laser welding, In High-Power Laser Materials Processing: Applications, Diagnostics, and Systems VI, San-Francisco, USA, 1009709

[14] Kogel-Hollacher, M., Schoenleber, M., Bautze, T., Strebel, M. & Moser, R. (2016) Measurement and closed-loop control of the penetration depth in laser materials processing, in 9th International Conference on Photonic Technologies LANE, Fürth, Germany.

[15] Kogel-Hollacher, M., André, S. & Beck, T. (2018) Low-coherence interferometry in laser processing: a new sensor approach heading for industrial applications, in Interferometry XIX, San Diego, USA 1074912.

[16] Dorsch, F., Harrer, T., Haug, P. & Plasswich, S. (2016) Process Control using capillary depth measurement, in 9th International Conference on Photonic Technologies LANE, Fürth, Germany,19-22.

[17] Schmoeller, M., Christian S., Liebl S. & Zaeh, M.F. (2018) In-Line Weld Depth Measurement for High Brilliance Laser Beam Sources Using Optical Coherence Tomography, in International Congress on Applications of Lasers & Electro-Optics (ICALEO), Orlando, USA, 502.

[18] Boley, M., Abt, F. & Weber, R. (2013), X-Ray and Optical Videography for 3D Measurement of Capillary and Melt Pool Geometry in Laser Welding, Physics Procedia, 41, 488–495.

[19] Vänskä, M., Abt, F., Weber, R. & Salminen, A. (2013) Effects of Welding Parameters Onto Keyhole Geometry for Partial Penetration Laser Welding, Physics Procedia, 41, 199–208

[20] Kaplan, A. (1994) A model of deep penetration laser welding based on calculation of the keyhole profile, Journal of Physics D: Applied Physics, 1805–1814.

[21] Aalderink, B.J., de Lange, D.F., Aarts, R.G.K.M. & Meijer, J. (2007) Keyhole shapes during laser welding of thin metal sheets, Journal of physics D: Applied physics, 40(17), 5388.

[22] Volpp, J. & Vollertsen, F. (2013) Analytical modeling of the keyhole including multiple reflections for analysis of the influence of different laser intensity distributions on keyhole geometry, Physics Procedia, 41, 460-468.

[23] Fixemer, P., Albert, F., Sievi, P. & Graham, T. (2015) Seam Guided Laser Remote Welding with Automated Gap Bridging: Increased process windows by online recognition of gap situation, Laser Technik Journal, 12(2), 38-41.

Meet the Authors

Dr Mikhail Sokolov is Research Fellow at Warwick Manufacturing Group (WMG), University of Warwick. He obtained his D.Sc. from Lappeenranta University of Technology, Finland, 2015 and worked at Luleå University of Technology, Sweden. He has published over 10 research papers. His focus is on laser beam welding, remote laser welding and methods for improving welding efficiency.

Dr Pasquale Franciosa is Associate Professor at WMG, University of Warwick - UK, and Visiting Professor at University of Naples - Italy. His focus is process monitoring, closed loop control, machine learning, multi-disciplinary optimization, with specific attention for automotive assembly systems and laser joining technology. He has published over 70 papers and received several best paper awards. Currently, he is responsible for the development of remote laser welding solutions to similar and dissimilar materials, with application to automotive body-in-white and battery systems. He serves on the editorial board of the ASTM SSME journal.

Dr Rehab Al Botros is Research Fellow at Warwick Manufacturing Group, University of Warwick. She obtained her PhD from the University of Warwick, 2015. Her background is in surface characterisation, imaging techniques and finite element method modelling. Her research focuses on manufacturing process monitoring and control, and characterisation of laser welding joints for quality improvement. She is author and co-author of several papers, published in international peer-reviewed journals.

Professor Darek Ceglarek is EPSRC Star Research Chair at University of Warwick and CIRP Fellow. Previously, he was Professor in Industrial and Systems Engineering at University of Wisconsin. His research focuses on digital manufacturing, in-process quality control and root cause analysis. He has published over 150 papers and received several Best Paper Awards. He served as Chair of the Quality, Statistics and Reliability Section of INFORMS; Program Chair for the ASME Design-for-Manufacturing Life Cycle Conferences, Associate Editor of the IEEE Trans. on Automation Science and Engineering, ASME Trans, Journal of Manufacturing Science & Engineering, ASTM Smart and Sustainable Manufacturing Systems.